



## ORIGINAL ARTICLE

# Sonochemical synthesis and characterization of CuInS<sub>2</sub> nanostructures using new sulfur precursor and their application as photocatalyst for degradation of organic pollutants under simulated sunlight



Aazam Jafarinejad <sup>a</sup>, Hadis Bashiri <sup>a,\*</sup>, Masoud Salavati-Niasari <sup>b,\*</sup>

<sup>a</sup> Department of Physical Chemistry, Faculty of Chemistry, University of Kashan, Kashan, Iran

<sup>b</sup> Institute of Nano Science and Nano Technology, University of Kashan, Kashan, P. O. Box. 87317-51167, Iran

Received 17 February 2022; accepted 23 May 2022

Available online 27 May 2022

## KEYWORDS

Nanostructures;  
Photodegradation;  
CuInS<sub>2</sub>;  
Erythrosine;  
Rubeanic acid;  
Sonochemical fabrication

**Abstract** In this research, we investigated the photocatalytic activity of CuInS<sub>2</sub> nanoparticles in visible light during the decomposition of three toxic dyes (Eriochrome Black T, Rhodamine B, and Erythrosine). The CuInS<sub>2</sub> nanostructures were synthesized by a rapid and simple sonochemical method using dithiooxamide as a sulfur reagent and various capping agents, including SDS, CTAB, and PVP, were applied to achieve a pure structure with fine morphology. The flower-like structure was observed through FESEM images, implying different capping agents and fabrication had a considerable influence on the morphology of samples. The suitable bandgap of CuInS<sub>2</sub> (1.53 eV) was obtained from DRS analysis and resulted in higher photodegradation efficiency. The fabricated CuInS<sub>2</sub> revealed better photodegradation efficiency (74.8%) to the anionic dyes than cationic dye. A possible photodegradation mechanism was suggested based on scavenger tests of active species.

© 2022 The Author(s). Published by Elsevier B.V. on behalf of King Saud University. This is an open access article under the CC BY-NC-ND license (<http://creativecommons.org/licenses/by-nc-nd/4.0/>).

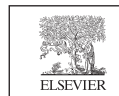
## 1. Introduction

Pure water is vital for life and has boosted needs because of the growth in the world population. While industrial settlement is beneficial to society, their emissions are composed of organic and inorganic sewage that impacts water quality and eventually concern the ecosystem and environment. In wastewater, non-biodegradable dyes cause aquatic contamination and have serious consequences (Phaltane et al., 2017; Liu et al., 2018; Thwin et al., 2019). Various biological, chemical, and physical water purification methods have been used to manage this issue but have failed because of enormous facility costs or the inability

\* Corresponding authors.

E-mail addresses: [hbashiri@kashanu.ac.ir](mailto:hbashiri@kashanu.ac.ir) (H. Bashiri), [Salavati@kashanu.ac.ir](mailto:Salavati@kashanu.ac.ir) (M. Salavati-Niasari).

Peer review under responsibility of King Saud University.



to complete the mineralization of these poisonous contaminants. The failure of these techniques has attracted the researcher's concentration on the evolution of new, simple, and inexpensive processes capable of complete wastewater purification (Rafique et al., 2018). Accordingly, photocatalytic activity based on the Advanced Oxidation Process (AOP) has evolved into a novel and promising technology with a significant ability to decompose inorganic and organic colorants. The photocatalytic revolution starts with the electron-hole ( $e^-h^+$ ) pair's production in response to light. This  $e^-h^+$  pairs are in charge of the reduction and oxidation procedures that destroy contaminants (Tahir et al., 2018).

Metal oxide semiconductors, including ZnO and TiO<sub>2</sub>, have been broadly employed as photocatalysts to degrade toxic pollutants in sewage because they are non-toxic and chemically and thermally stable (Ong et al., 2018; Jiang et al., 2020). Unfortunately, these compounds have the problem of low visible light utilization because of the wide bandgap (3.3 eV for ZnO and 3.2 eV for TiO<sub>2</sub>) (Ong et al., 2018; Schneider et al., 2014). Binary metal sulfides are alluring nominees as positively efficient photocatalysts driven by visible light. Since the valence bands of these compounds are composed of 3p orbitals of S, the bandgap is narrower than those of metal oxides and therefore sensitizes the majority of metal sulfides to visible rays (Haque et al., 2018). Nevertheless, these compounds possess low efficiency of charge separation and suffer from photo corrosion, restricting their functional usages (Zhang and Zhu, 2010). Lately, photocatalysts based on ternary metal sulfide have been highly emphasized in photocatalysis investigation due to their long-term corrosion resistance, high thermal property, and high absorption coefficient over a broad spectral range in comparison with photocatalysts based on binary metal sulfide (Regulacio and Han, 2016; Yousif and Agbolaghi, 2020). Intriguingly, nanostructured photocatalysts with high specific surface areas have more active locations for the optimal transfer of  $e^-$  and  $h^+$  to the photocatalyst surface that are obtainable for photocatalytic reactions. All of this leads to improved photocatalytic behavior compared to bulk structures (Adhikari and Lachgar, 2016).

A promising ternary metal sulfide is copper indium sulfide (CuInS<sub>2</sub>), which has a variety of potential uses, such as photodetectors, photocatalysis, solar cells, and bioimaging (Bulyarsky et al., 2016; Jabarullah et al., 2019; Haran and Yousif, 2022; Zhang et al., 2020; Liu et al., 2013; Deng et al., 2012). Its valence band is made of 3p orbitals from S, and its conduction band is composed of 5 s orbitals from In (Regulacio and Han, 2016). Therefore, the narrower bandgap (1.53 eV) can be obtained (Luo et al., 2015). CuInS<sub>2</sub> has been studied as a photocatalyst for reduction of nitrate ion (Haran and Yousif, 2022), H<sub>2</sub> generation (Kobayakawa et al., 1992), and decomposition of toxic pollutants (Liu et al., 2011; Yousif and Al-Zhara, 2016). Hydro/solvothermal approaches have been applied to fabricate CuInS<sub>2</sub> nanostructures (Han et al., 2009; Yousif and Haran, 2021). Nevertheless, these techniques commonly demand high electrical energy consumption, extended reaction time, and complicated and expensive tools. The sonochemical approach plays an important role in the nanostructure preparation with small crystal sizes and high surface areas. This is a property that is helpful for photocatalytic performance (Karami et al., 2021). The sonochemical procedure is an efficient technique for the fabrication of nanostructures over a brief reaction time because of its high potential to pulse, which can create hot spots in the reaction media (Ghanbari and Salavati-Niasari, 2018).

In this work, we utilized a sonochemical approach to produce CuInS<sub>2</sub> nanostructures employing dithiooxamide (also known as rubeanic acid) as a sulfur precursor. Dithiooxamide is an organic compound. It is the sulfur analog of oxamide. It performs as a chelating agent, for example, in the determination or detection of copper. Besides, it has been utilized as a construction unit in the fabrication of cyclen (Soylak and Erdogan, 2006). To our knowledge, this is the first time that rubeanic acid has been used as a sulfur precursor. The types of capping agents, including SDS, CTAB, and PVP, were investigated on the purity and morphology of CuInS<sub>2</sub> nanostructures.

According to the Tauc plot, CuInS<sub>2</sub> has a proper bandgap in the visible region (1.53 eV). Therefore, the photodegradation behavior of Eriochrome Black T (ECBT), Rhodamine B (RhB), and Erythrosine (Ery) (denoting toxic contaminants) with respect to the fabricated CuInS<sub>2</sub> photocatalyst was scrutinized. The possible photodegradation mechanism was carried out through scavenger experiments of active species.

## 2. Experimental

### 2.1. Precursors

All precursors involved in this study were of analytical grade and utilized as obtained with no additional refinement. Copper nitrate trihydrate (Cu(NO<sub>3</sub>)<sub>2</sub>·3H<sub>2</sub>O), Propylene glycol (PG), Sodium dodecyl sulfate (SDS), Indium chloride (InCl<sub>3</sub>), Polyvinylpyrrolidone (PVP), Ethylenediaminetetraacetic acid (EDTA), Rubeanic acid, Methanol, 1,4-Benzoquinone (BQ), Cetyltrimethylammonium bromide (CTAB), and Benzoic acid (BA) were procured from Sigma-Aldrich.

### 2.2. Preparation of CuInS<sub>2</sub> nanostructures

In a standard approach, CuInS<sub>2</sub> was synthesized by combining InCl<sub>3</sub>, Cu(NO<sub>3</sub>)<sub>2</sub>, rubeanic acid, and surfactant, including SDS, PVP, and CTAB under ultrasonic radiation. 0.62 mmol Cu(NO<sub>3</sub>)<sub>2</sub> was dissolved in 10 mL PG, 1.24 mmol surfactant was liquified in 10 mL PG and added to Cu<sup>2+</sup> solution. In the next step, 0.61 mmol InCl<sub>3</sub> was dissolved in 10 mL propylene glycol and added to the mentioned solution. 1.24 mmol rubeanic acid was also dissolved in 10 mL propylene glycol and added to the mixture under ultrasonic radiation for 10 min. The obtained dark brown powder was washed with ethyl alcohol and dionized water multiple times and dried at 70 °C for 12 h. The dried powder was annealed at 400 °C for 2 h in a gas mixture of 85% Argon and 15% Hydrogen. Table 1 and Scheme 1 show the different condition for fabrication of CuInS<sub>2</sub>.

### 2.3. Photocatalytic process

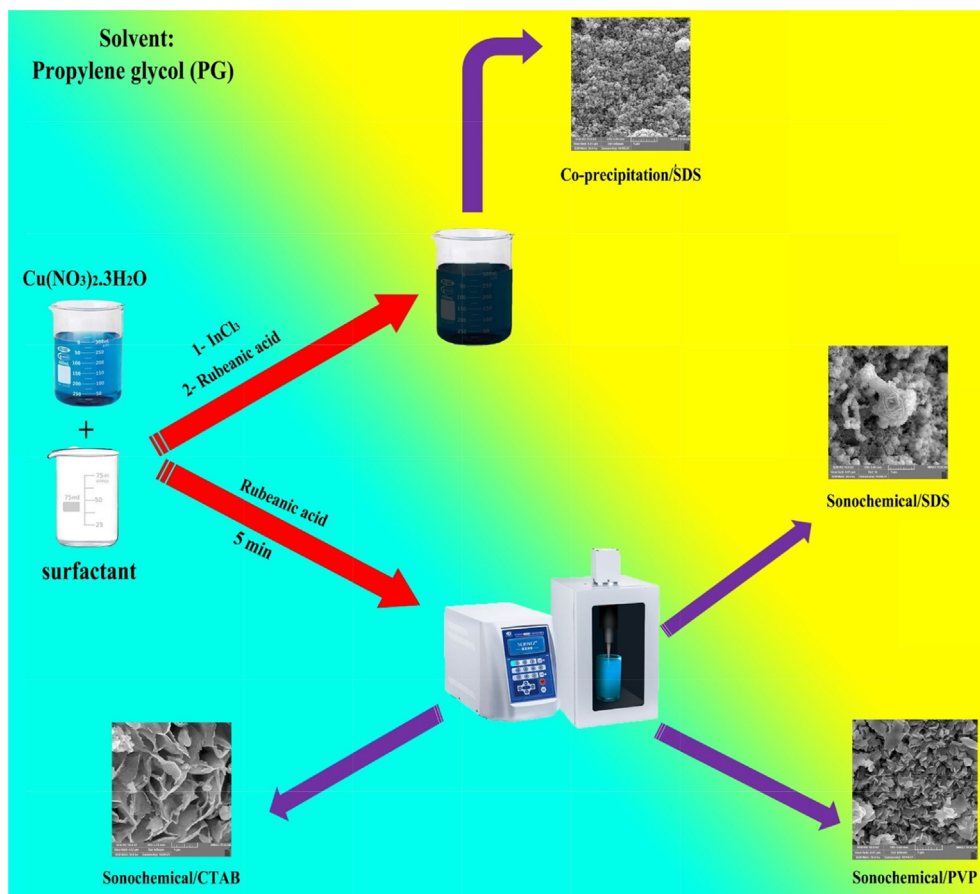
CuInS<sub>2</sub> was used to examine its photocatalytic activity for decolorization of toxic colorants, including Eriochrome Black T, Rhodamine B, and Erythrosine under visible light. A 150 W Osram lamp with a wavelength between 400 and 780 nm was used as the radiation source for the photocatalytic operation. The tests were run without radiation and CuInS<sub>2</sub>, and virtually no dye was eliminated after 2 h. In each experiment, 20 mg of CuInS<sub>2</sub> was added to 20 mL of 10 ppm toxic contaminate. The suspension was agitated in the darkness for 0.5 h before activating the visible lamp. A 3 mL specimen was taken from the mixture every 15 min throughout radiance and centrifuged at 11,000 rpm for 6 min. Buoyancy was gathered, filtered, and monitored with a UV-Vis spectrophotometer.

## 3. Result and discussion

### 3.1. Characterization

FT-IR spectra of CuInS<sub>2</sub> before and after annealing, and rubeanic acid are illustrated in Fig. 1. FTIR spectroscopy

Sample No.	Surfactant	Method	In: Cu: Surfactant	Grain size (nm)
1	SDS	Co-precipitation		18.43
2	CTAB		1:1:2	16.96
3	SDS	Sonochemical		17.31
4	PVP			19.00



**Scheme 1** Schematic of preparation of CuInS<sub>2</sub> by sonochemical method.

was employed to verify the existence of the chemical structure of CuInS<sub>2</sub>. The FTIR spectra indicate the lack of lattice vibrations generated with CuInS<sub>2</sub> in the 4000–400 cm<sup>-1</sup> spectral range. Nevertheless, it reveals vibrations at 1271 and 621 cm<sup>-1</sup> can be associated with the sulfate group (SO<sub>4</sub>) (Adhikari and Lachgar, 2016). The FTIR information in annealed CuInS<sub>2</sub> reduces as compared to un-annealed CuInS<sub>2</sub>. Absorption bands at 3439 cm<sup>-1</sup> and 3238 cm<sup>-1</sup> indicate the existence of both indium and copper complexes. This Figure also reveals the characteristic peak at 1271 cm<sup>-1</sup>, which are designated to CuSO<sub>4</sub>. The absorption band at 782 cm<sup>-1</sup> belongs to the Cu<sub>2</sub>O group (Behera et al., 2013). The IR spectra demonstrated the potential vibration at 3228 cm<sup>-1</sup>, which belonged to the existence of both indium and copper. The vibration peaks at 1052 and 864 cm<sup>-1</sup> for Cu-complex and In-complex because of C=S stretching vibrations (Bera

et al., 2008). Besides, the absorption bands at 1631 cm<sup>-1</sup>, 1509 cm<sup>-1</sup> belong to CuS (Krunks et al., 2002). The absorption bands of rubenic acid (Fig. 3c), including 3294, 3134, 1585, 1427, 1278, 1195, 835, 705, and 639 cm<sup>-1</sup>, were so identical to the peaks documented in the literature (Hinogami et al., 2012).

The XRD patterns for specimens 1–4 were presented in Fig. 2(a–d). The XRD pattern of specimen 1 prepared by the co-precipitation method (Fig. 2a) shows an impurity such as Cu<sub>2</sub>S (JCPDS No. 072-1071) in the final product. Fig. 2(b–d) unveils the XRD patterns of CuInS<sub>2</sub> synthesized by sonochemical method in the presence of three different types of capping agents, including CTAB (cationic), SDS (anionic), and PVP (polymeric), respectively. Sample 2 (Fig. 2b) was formed from CuInS<sub>2</sub> with JCPDS No. 38-0777 as the main product and Cu<sub>2</sub>S (JCPDS No. 072-1071) as an impurity. Fig. 2c and 2d

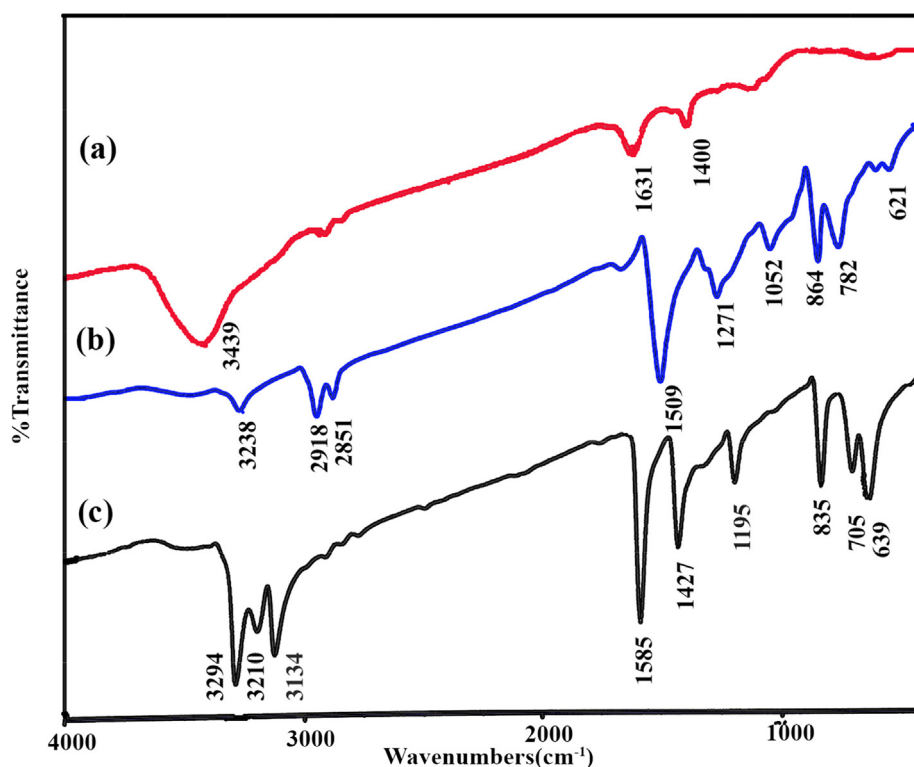


Fig. 1 FTIR spectra of CuInS<sub>2</sub> (a) before, (b) after annealing, and (c) Rubenic acid.

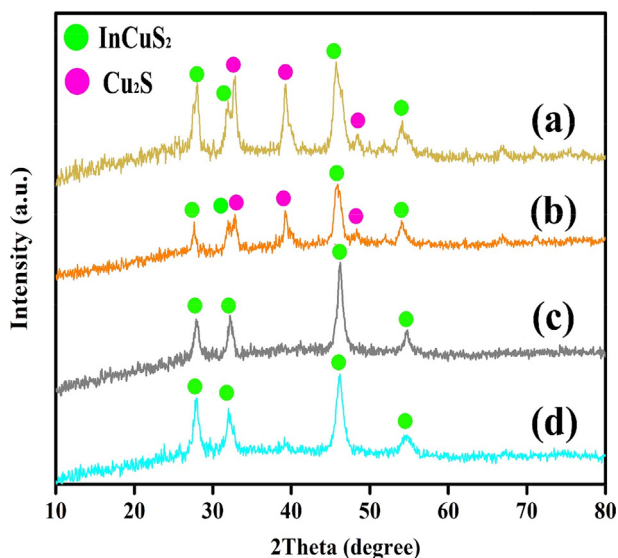


Fig. 2 XRD patterns of CuInS<sub>2</sub> (a) Sample 1 (Co-precipitation/SDS), (b) Sample 2 (Sonochemical/CTAB), (c) Sample 3 (Sonochemical/SDS), (d) Sample 4 (Sonochemical/PVP).

were allocated to the tetragonal phase of CuInS<sub>2</sub> with reference code of JCPDS No. 38-0777 ( $a = b = 5.5200 \text{ \AA}$ , and  $c = 11.1200 \text{ \AA}$ ) and space group of I-42d. The diffraction peaks in these patterns correspond to the (112), (211), (200), (220), and (316) planes. There are no diffraction peaks related to other phases in Fig. 2c and 2 d, suggesting the acquired product in the presence of SDS and PVP (samples

3 and 4) are pure, while the XRD patterns of the sample achieved in the presence of CTAB (specimen 2) indicated the existence of some impurity like Cu<sub>2</sub>S (072-1071) in the final product. Scherrer equation was applied to estimate the grain size in the range of 16–19 nm (Table 1) (Abkar et al., 2022).

$$D = K\lambda/\beta\cos\theta \quad (1)$$

The corresponding reaction to compose stoichiometric CuInS<sub>2</sub> during the sonochemical procedure can be presented as follow:

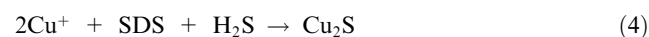
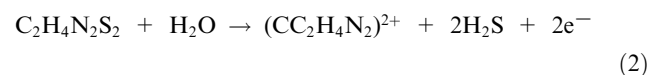
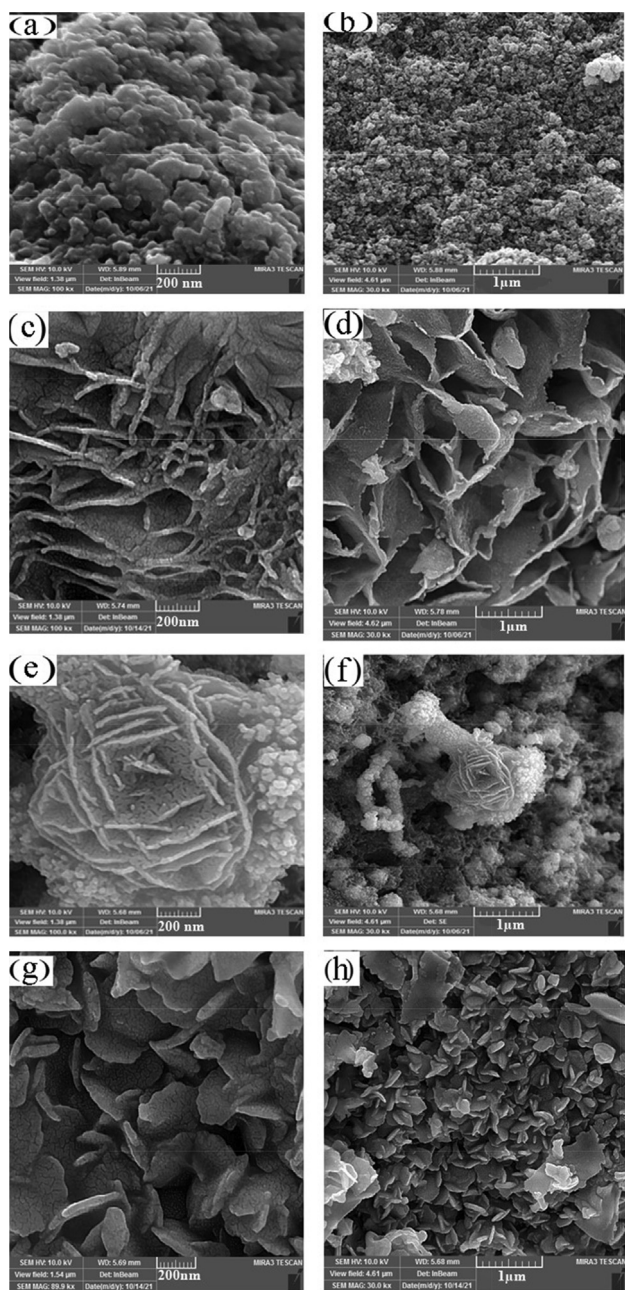


Fig. 3 indicates the SEM images of the CuInS<sub>2</sub>. Fig. 3a and b illustrates that the co-precipitation method results in a large amount of sphere-like nanoparticles with agglomeration. Fig. 3c and d shows the SEM images of CuInS<sub>2</sub> in the existence of CTAB as a cationic covering agent, representing homogeneous flake-like particles. Flower-like morphology was observed for CuInS<sub>2</sub> utilizing SDS as an anionic surfactant (Fig. 3e and f). Applying PVP as a polymeric surfactant was composed flake structures of CuInS<sub>2</sub>. The particle size of the CuInS<sub>2</sub> is between 11 and 14 nm based on the TEM image



**Fig. 3** FE-SEM images of the CuInS<sub>2</sub> (a,b) Sample 1 (Cociprecipitation/SDS), (c,d) Sample 2 (Sonochemical/CTAB), (e,f) Sample 3 (Sonochemical/SDS), (g,h) Sample 4 (Sonochemical/PVP).

of the CuInS<sub>2</sub> (sample 3, Fig. 4). The EDS spectrum of CuInS<sub>2</sub> (specimen 3) shows that the compound is composed of Cu, In, and S elements without any impurities (Fig. 5).

The surface characterization of CuInS<sub>2</sub> nanostructures is illustrated in Fig. 6. The received isotherm is type III with H3-type hysteresis (Fig. 6a), belonging to the mesoporous materials. The average size of pores was obtained between 1 and 25 nm for sample 3 from the BJH plot (Fig. 6b). The specific surface area is 11.96 m<sup>2</sup>/g, the pore size on average, and the total pore volume is 6.77 nm and 0.024 cm<sup>3</sup>/g, respectively.

The optical property of CuInS<sub>2</sub> (sample 3) is indicated in Fig. 7 using UV-Vis diffuse reflectance spectroscopy (DRS). CuInS<sub>2</sub> shows typical absorptions in the area of 200–500 nm. The optical bandgap (B.G.) was calculated by (Ghanbari and Salavati-Niasari, 2018),

$$A(h\nu - \text{B.G.}) = (\alpha h\nu)^{1/n} \quad (7)$$

which  $n$  is 1/2 or 2 for direct and indirect bandgap,  $A$  is a material constant,  $\alpha$  is absorption factor, and  $h\nu$  is the light energy, respectively (Ghanbari and Salavati-Niasari, 2018). The bandgap was obtained at 1.53 eV for CuInS<sub>2</sub>, making it convenient for photocatalytic application in the visible area.

### 3.2. Photocatalytic performance

The photocatalytic behavior of CuInS<sub>2</sub> (sample 3) was examined by observing the decolorization of three different dyes, including Eriochrome Black T, Rhodamine B, and Erythrosine in an aqueous solution, below visible light (Fig. 8). With no irradiation or CuInS<sub>2</sub>, nearly no dyes were decolorized after 120 min revealing the self-decolorization was inapplicable. The decolorization percentage (%D) was calculated as

$$\%D = (A_0 - A_t)/A_0 \times 100 \quad (8)$$

which  $A_0$  and  $A_t$  are absorbance of the sample solution before and after degradation, respectively (Orooji et al., 2020). The influence of three different pollutants and the catalyst dosages (0.01, 0.02, and 0.03 g) was accomplished to attain adequate efficiency. Fig. 8a reveals the photocatalytic decolorization of 0.02 g CuInS<sub>2</sub> in the presence of Eriochrome Black T, Rhodamine B, and Erythrosine. These dyes were decolorized about 59.7%, 53.2%, and 74.8% after 120 min, respectively. Fig. 8b unveils the impact of CuInS<sub>2</sub> dosages on the decolorization of Erythrosine. Increasing CuInS<sub>2</sub> dosage from 0.01 to 0.02 g has enhanced the decolorization of Erythrosine from 52.0% to 74.8%, while enhancing dosage from 0.02 to 0.03 g has resulted in a reduction from 74.8% to 65.6%. Hence, enriching the CuInS<sub>2</sub> doses improve the surface of the catalyst and improves the adsorption of dye on the CuInS<sub>2</sub> surface. Nevertheless, the expansion in the catalyst dosage is practical up to a specific quantity (0.02 g), and then CuInS<sub>2</sub> saturation layers were observed. Increasing the thickness of CuInS<sub>2</sub> in the colorant solution averts radiation from reaching the solution and reduces the efficiency (Sunayana et al., 2010). Fig. 8b demonstrates the impact of pollutant concentrations (10 and 15 ppm) of Erythrosine after 120 min, unveiling that increasing concentration from 10 ppm to 15 ppm reduces the decolorization from 74.8% to 60.7%. Fig. 9a shows the effect of Cu<sub>2</sub>S as an impurity in the photocatalytic efficiency, which indicates that the decolorization performance indicates an obvious reduction (29.2%). Table 2 lists the photocatalytic activates of some sulfide compounds in comparison with CuInS<sub>2</sub>. The results show that CuInS<sub>2</sub> are a potential photocatalyst and it can compete with other related compounds for water treatment.

Three different scavengers, including BQ for O<sub>2</sub><sup>-</sup>, EDTA for h<sup>+</sup>, and (BA) for ·OH, were used to remove the essential influential factors to evaluate the impact of active species in the photodecolorization of toxic pollutants (Mahdiani et al., 2018). As shown in Fig. 9b, the photodecolorization was scar-

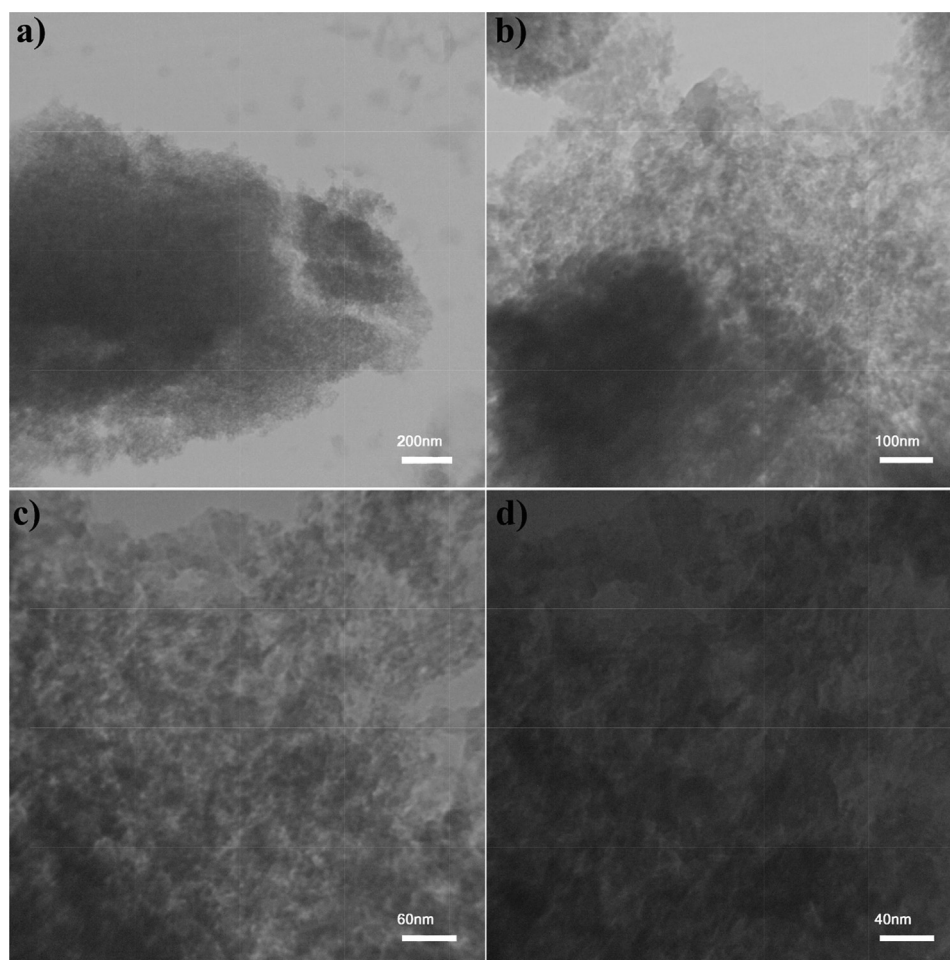


Fig. 4 TEM images of CuInS<sub>2</sub> Sample 3.

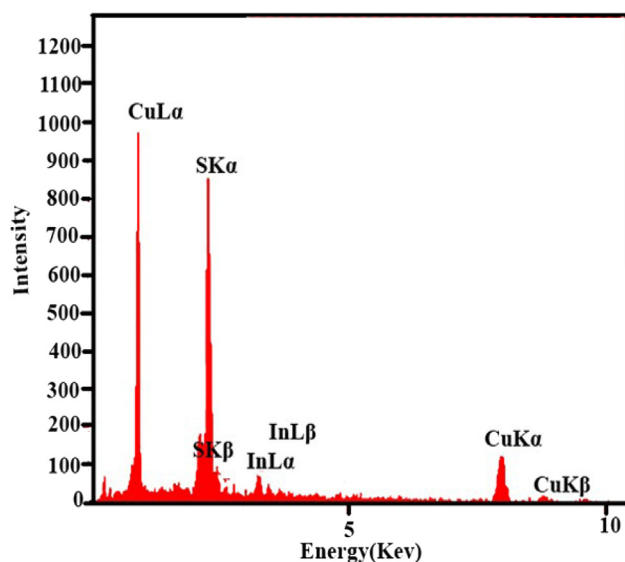


Fig. 5 EDS spectrum of Sample 3.

cely decreased with the addition of 1,4-Benzoquinone as no scavenger was used. Regardless, when Benzoic acid and EDTA were used to remove  $\cdot\text{OH}$  and  $h^+$ , a notable decrease in photocatalytic efficiency was observed, which confirmed the influence of  $\cdot\text{OH}$  and  $h^+$  on the photo-oxidation approach. In summary, the impacts of diverse scavengers showed that  $\cdot\text{OH}$  and  $h^+$  recreated prominent parts, and  $\text{O}_2^{\cdot-}$  recreated an insignificant part in Erythrosine decolorization. It is well established that the electrons of the conduction band (CB) and holes of the valence band (VB) are formed when the aqueous suspension of the catalyst is irradiated with light energy higher than its bandgap (1.53 eV) (Tang et al., 2014). The photogenerated electrons can reduce dye or react with electron acceptors, such as dissolved  $\text{O}_2$  in water or adsorbed on the surface of a catalyst and reduced it to  $\text{O}_2^{\cdot-}$  (superoxide anion radical). The photogenerated holes can react with  $\text{H}_2\text{O}$  or  $\text{OH}^-$  and oxidize them into  $\text{OH}^{\cdot}$  radicals or oxidize the organic dyes to produce  $\text{R}^+$ . They have been reported to be responsible for the photodegradation of organic dyes together with other high oxidant species (peroxide radicals). Several previous studies have reported on several reactions that take place in a photocatalytic process

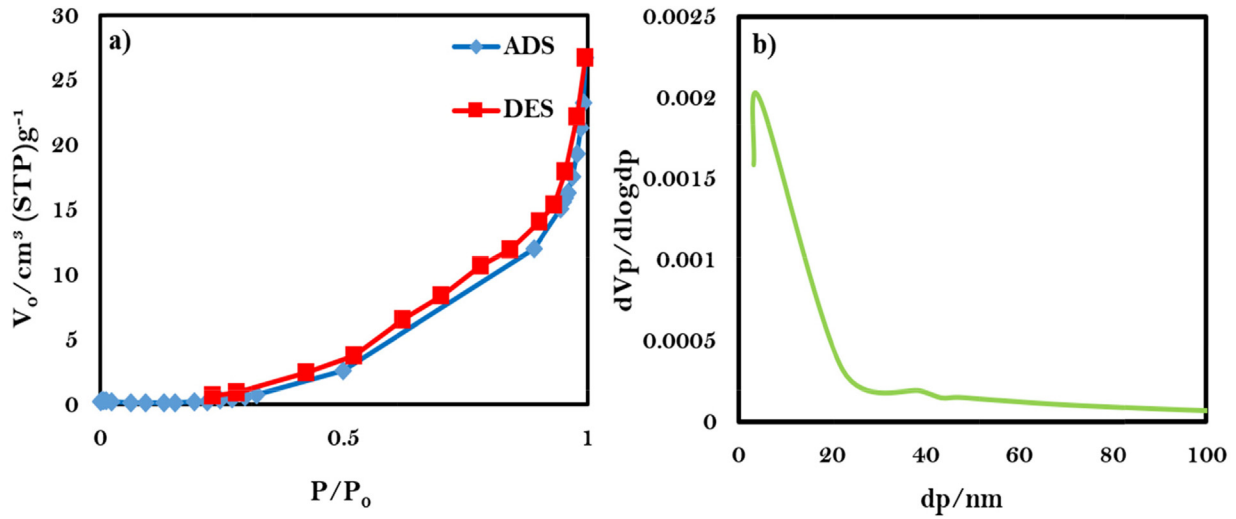


Fig. 6 (a) Low temperature N<sub>2</sub> adsorption/desorption isotherm, (b) BJH plot of CuInS<sub>2</sub> nanostructures (sample 3).

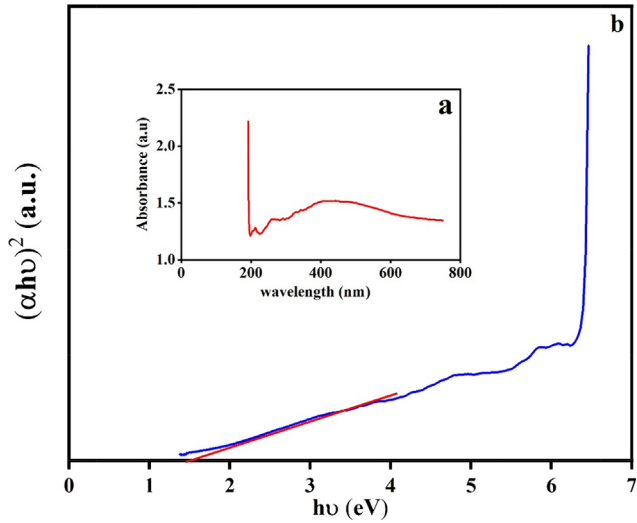
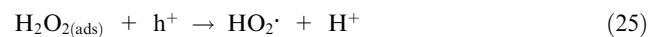
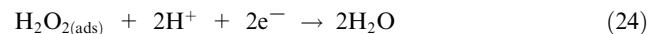
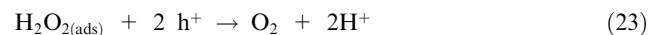
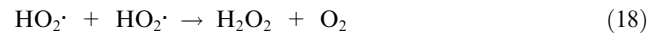
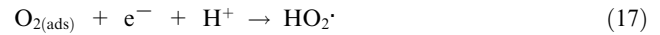
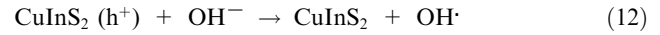
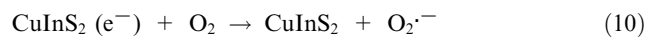
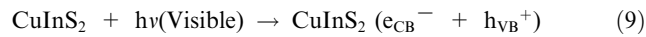


Fig. 7 UV-vis absorption spectrum and the corresponding plots of  $(\alpha h\nu)^2$  against photon energy ( $h\nu$ ) of CuInS<sub>2</sub>.

and involve H<sub>2</sub>O<sub>2</sub>, ·OH and O<sub>2</sub><sup>·-</sup>. Thus, the connected reactions at the CuInS<sub>2</sub> surface driving the dye decolorization can be described as follows (Konstantinou and Albanis, 2004; Arabameri and Bashiri, 2021; Arabameri and Bashiri, 2022; Mohammed and Yousif, 2021; Yousif, 2021; Abdulsahib et al., 2021; Aljeboree et al., 2020; Aljeboree et al., 2021; Alshamusi et al., 2021; Ganduh et al., 2021; Ganduh et al., 2021; Jasim et al., 2022; Mahdi et al., 2021):



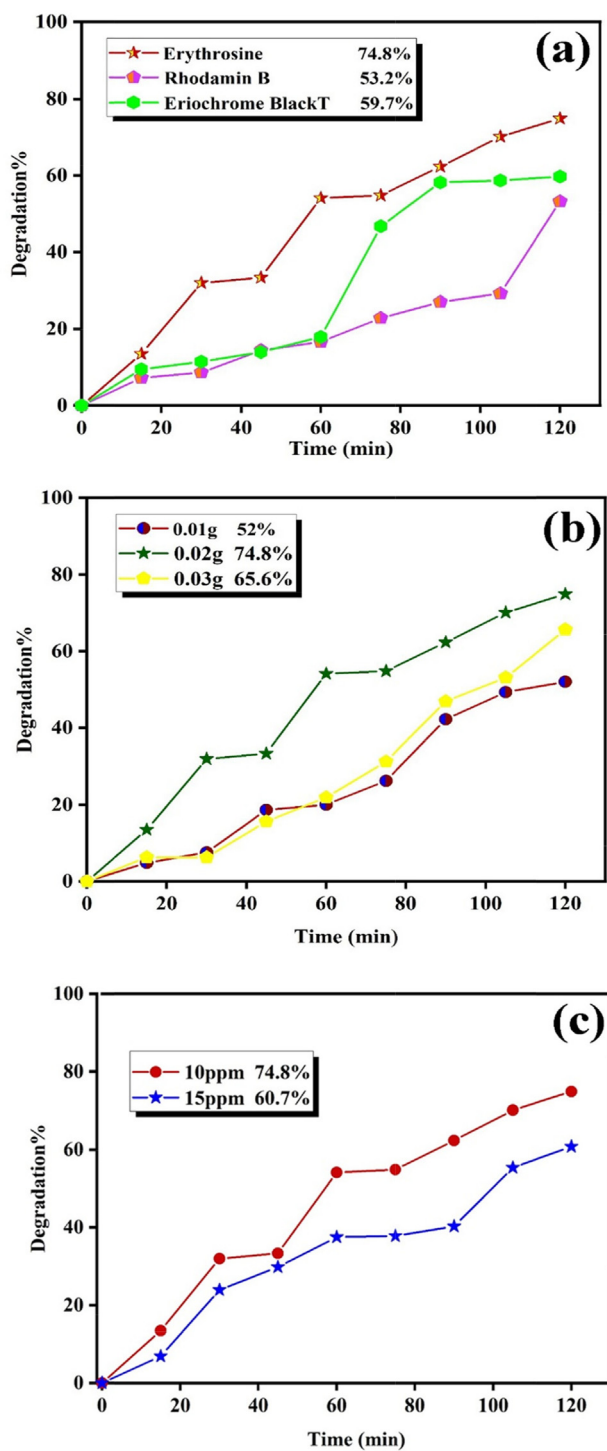


Fig. 8 Photodecolorization of CuInS<sub>2</sub> (a) over three different dyes, (b) catalyst dosages over Erythrosine, and (c) Erythrosine concentrations.

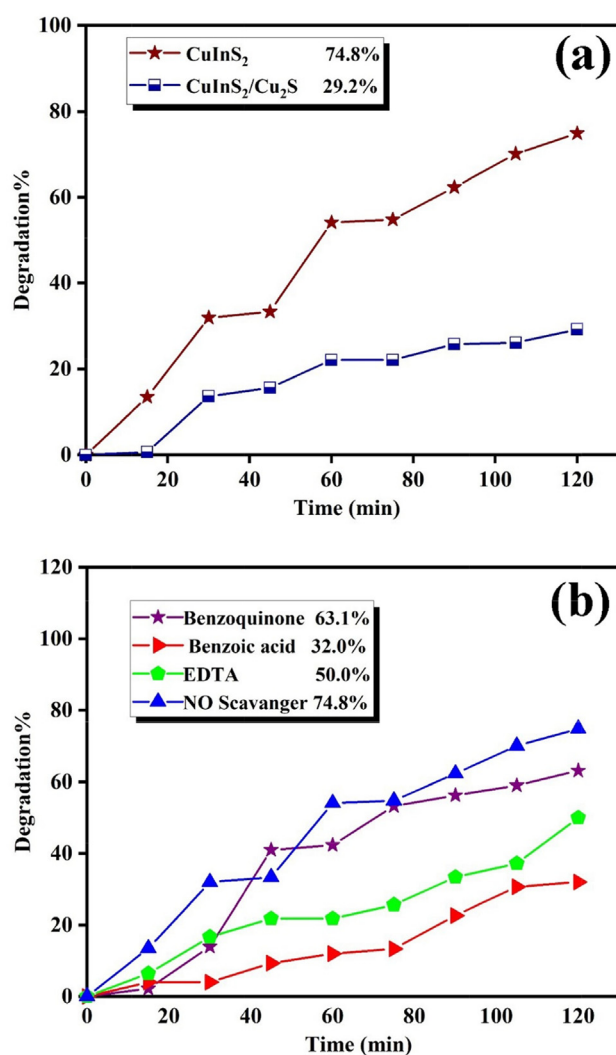
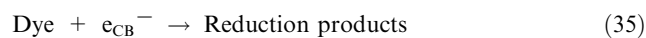
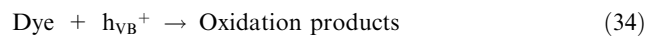
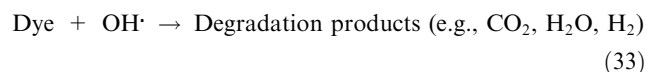
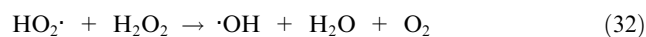
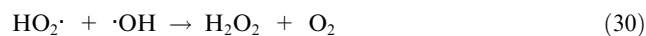


Fig. 9 Photodecolorization of (a) CuInS<sub>2</sub> and CuInS<sub>2</sub>/Cu<sub>2</sub>S, and (b) scavenger test over Erythrosine.



**Table 2** Photocatalytic activity of sulfide compounds.

Sample	Highest decolorization (%)	Lowest decolorization (%)	Catalyst dosage (g)	Source of light	Ref.
CuInS <sub>2</sub> nanostructures	74.8 (Ery)	53.2 (RhB)	0.02	Vis	This work
ZnIn <sub>2</sub> S <sub>4</sub> /CdIn <sub>2</sub> S <sub>4</sub> nanocomposite	100 (RhB)	99.7 (MO*)	0.04	Vis	Mahdi et al., 2021
PS/ZnIn <sub>2</sub> S <sub>4</sub> nanocomposites	86 (MO)	–	0.02	Vis	Sun et al., 2017
CdIn <sub>2</sub> S <sub>4</sub> nanostructures	98 (MO)	–	0.05	Vis	Yuan et al., 2020
ZnS/CdIn <sub>2</sub> S <sub>4</sub> nanocomposite	71 (RhB)	–	0.05	Vis	Mu et al., 2012
ZnS-ZnIn <sub>2</sub> S <sub>4</sub> nanocomposites	97 (MB**)	34 (MB)	0.01	UV	Xu et al., 2013
CDs@-ZnIn <sub>2</sub> S <sub>4</sub>	100 (MO)	–	0.05	Vis	Janani et al., 2021
CuInS <sub>2</sub> nanostructures	74.29 (RhB)	64.08 (MB)	0.1	Vis	Lei et al., 2019
CuInS <sub>2</sub> nanostructures	65 (RhB)	–	0.1	Vis	Chumha et al., 2020

\* Methyl Orange.

\*\* Methylene Blue.

@ Carbon Nanodots.

#### 4. Conclusions

Pure and flower-like CuInS<sub>2</sub> nanostructures were fabricated by a facile and rapid sonochemical procedure utilizing dithiooxamide as a sulfur reagent and various capping agents, including SDS, and PVP, which only demanded 10 min of ultrasonic irradiation. CuInS<sub>2</sub> exhibited higher photocatalytic performance on Erythrosine than on two other dyes, which was ascribed to the electrostatic interaction between Erythrosine molecules and the positive charge on the surface of CuInS<sub>2</sub>. The scavenger tests revealed that h<sup>+</sup> and ·OH were responsible for the photodecolorization operation. The outcomes implied that the CuInS<sub>2</sub> nanostructures could be a potential photocatalyst for the decolorization of toxic contaminants in sewage below visible rays. Besides, the sonochemical technique is desired to apply to the fabrication of other ternary chalcogenide nanostructures.

#### CRedit authorship contribution statement

**Aazam Jafarnejad:** Investigation, Formal analysis, Methodology, Writing – original draft, Software. **Hadis Bashiri:** Supervision, Project administration, Validation, Resources. **Masoud Salavati-Niasari:** Formal analysis, Methodology, Writing – review & editing, Writing – original draft, Conceptualization, Supervision, Project administration, Investigation, Data curation, Validation, Resources, Visualization, Funding acquisition.

#### Declaration of Competing Interest

The authors declare that they have no known competing financial interests or personal relationships that could have appeared to influence the work reported in this paper.

#### Acknowledgement

The authors acknowledge the University of Kashan by Grant No (159271/AJ1 and 1143438/1) and Iran National Science Foundation (INSF, 97017837) for supporting this investigation.

#### References

- Abdulsahib, W.K., Sahib, H.H., Mahdi, M.A., Jasim, L.S., 2021. Adsorption Study of Cephalexin Monohydrate Drug in Solution on Poly (vinyl pyrrolidone-acryl amide) Hydrogel Surface. *Int. J. Drug Delivery Technol.* 11 (4), 1169–1172. <https://doi.org/10.25258/ijddt.11.4.9>.
- Abkar, E., Izadi, E., Amiri, O., Ghanbari, M., Salavati-Niasari, M., 2022. Sonochemical synthesis and characterization of Cu<sub>2</sub>HgI<sub>4</sub> nanostructures photocatalyst with enhanced visible light photocatalytic ability. *Arabian J. Chem.* 15, 103536.
- Adhikari, S., Lachgar, A., 2016. Effect of particle size on the photocatalytic activity of BiNbO<sub>4</sub> under visible light irradiation. *J. Phys.: Conf. Ser.: IOP Publish.* 012017
- Aljeboree, A.M., Alrazzak, N.A., Alqaraguly, M.B., Mahdi, M.A., Jasim, L.S., Alkaim, A.F., 2020. Adsorption of pollutants by using low-cost (Environment-Friendly): Equilibrium, kinetics and thermodynamic studies: A review. *System. Rev. Pharm.* 11 (12), 1988–1997. <https://doi.org/10.31838/srp.2020.12.303>.
- Aljeboree, A.M., Mohammed, R.A., Mahdi, M.A., Jasim, L.S., Alkaim, A.F., 2021. Synthesis, characterization of p(Ch/aa-co-am) and adsorptive removal of pb(ii) ions from aqueous solution: Thermodynamic study. *NeuroQuantology* 19 (7), 137–143. <https://doi.org/10.14704/nq.2021.19.7.NQ21096>.
- Alshamusi, Q.K.M., Alzayd, A.A.M., Mahdi, M.A., Jasim, L.S., Aljeboree, A.M., 2021. Adsorption of crystal violet (CV) dye in aqueous solutions by using P(PVP-co-AAM)/go composite as (eco-healthy adsorbate surface): characterization and thermodynamics studies. *Biochem. Cell. Archiv.* 21, 2423–2431.
- Arabameri, M., Bashiri, H., 2021. Introduction of the Effective Photon Concentration Variable for Studying the Mechanism of Crystal Violet Photodegradation. *Photochem. Photobiol.*
- Arabameri, M., Bashiri, H., 2022. A new approach to study the degradation of the organic pollutants by A-doped MxOy/B photocatalysts. *Environ. Sci. Pollut. Res.*, 1–25
- Behara, P.S., Rajesh, D., Karthikeyan, S., Sunandana, C., Mohan, D. B., 2013. Single Phase Formation of CuInS<sub>2</sub> Nanoparticles: Structural, Morphological, Thermal Studies with Annealing Effect. *J Appl Phys.*, 4–6
- Bera, P., Kim, C.-H., Seok, S.I., 2008. Synthesis, spectroscopic characterization and thermal behavior of cadmium (II) complexes of S-methylthiocarbamate (SMDTC) and S-benzylthiocarbamate (SBDTC): X-ray crystal structure of [Cd (SMDTC) 3]· 2NO<sub>3</sub>. *Polyhedron* 27, 3433–3438.

- Bulyarsky, S., Vostretsova, L., Gavrilov, S., 2016. Photodetectors based on CuInS<sub>2</sub>. *Semiconductors* 50, 106–111.
- Chumha, N., Pudkon, W., Chachvalvutikul, A., Luangwanta, T., Randorn, C., Inceesungvorn, B., et al, 2020. Photocatalytic activity of CuInS<sub>2</sub> nanoparticles synthesized via a simple and rapid microwave heating process. *Mater. Res. Express* 7, 015074.
- Deng, D., Chen, Y., Cao, J., Tian, J., Qian, Z., Achilefu, S., et al, 2012. High-quality CuInS<sub>2</sub>/ZnS quantum dots for in vitro and in vivo bioimaging. *Chem. Mater.* 24, 3029–3037.
- Ganduh, S.H., Kmal, R.Q., Mahdi, M.A., Aljeboree, A.M., Jasim, L.S., 2021. Selective spectrophotometric determination of 4-amino antipyrine antibiotics in pure forms and their pharmaceutical formulations. *Int. J. Drug Delivery Technol.* 11 (2), 371–375. <https://doi.org/10.25258/ijddt.11.2.23>.
- Ganduh, S.H., Aljeboree, A.M., Mahdi, M.A., Jasim, L.S., 2021. Spectrophotometric Determination of Metoclopramide-HCL in the Standard Raw and it Compared with Pharmaceuticals. *J. Pharm. Negative Results* 12 (2), 44–48. <https://doi.org/10.47750/pnr.2021.12.02.008>.
- Ghanbari, M., Salavati-Niasari, M., 2018. Ti<sub>4</sub>CdI<sub>6</sub> nanostructures: facile sonochemical synthesis and photocatalytic activity for removal of organic dyes. *Inorg. Chem.* 57, 11443–11455.
- Han, S., Kong, M., Guo, Y., Wang, M., 2009. Synthesis of copper indium sulfide nanoparticles by solvothermal method. *Mater. Lett.* 63, 1192–1194.
- Haque, F., Daeneke, T., Kalantar-Zadeh, K., Ou, J.Z., 2018. Two-dimensional transition metal oxide and chalcogenide-based photocatalysts. *Nano-micro Lett.* 10, 1–27.
- Haran, N.H., Yousif, Q.A., 2022. The efficiency of TiO<sub>2</sub> nanotube photoanode with graphene nanoplatelets as counter electrode for a dye-sensitized solar cell. *Int. J. Ambient Energy* 43, 1–8. <https://doi.org/10.1080/01430750.2019.1636880>.
- Hinogami, R., Yotsuhashi, S., Deguchi, M., Zenitani, Y., Hashiba, H., Yamada, Y., 2012. Electrochemical reduction of carbon dioxide using a copper rubeanate metal organic framework. *ECS Electrochem. Lett.* 1, H17.
- Jabarullah, N.H., Razavi, R., Hamid, M.Y., Yousif, Q.A., Najafi, M., 2019. Potential of Ge-adopted Boron Nitride Nanotube as Catalyst for Sulfur Dioxide Oxidation. *Prot. Met. Phys. Chem* 55, 671–676. <https://doi.org/10.1134/S2070205119040129>.
- Janani, R., Melvin, A.A., Singh, S., 2021. Facile one pot in situ synthesis of ZnS–ZnIn<sub>2</sub>S<sub>4</sub> composite for improved photocatalytic applications. *Mater. Sci. Semicond. Process.* 122, 105480.
- Jasim, L.S., Aljeboree, A.M., Sahib, I.J., Mahdi, M.A., Abdulrazzak, F.H., Alkaim, A.F., 2022. Effective adsorptive removal of riboflavin (RF) over activated carbon. *AIP Conf. Proc.* 2386 (2022), 030030. <https://doi.org/10.1063/5.0066996>.
- Jiang, N., Ebadi, A.G., Kishore, K.H., Yousif, Q.A., Salmani, M., 2020. Thermomechanical reliability assessment of solder joints in a photovoltaic module operated in a hot climate. *IEEE Trans. Compon., Packag. Manuf. Technol.* 10, 160–167. <https://doi.org/10.1109/TCPMT.2019.2933057>.
- Karami, M., Ghanbari, M., Amiri, O., Ghiyasiyan-Arani, M., Salavati-Niasari, M., 2021. Sonochemical synthesis, characterization and investigation of the electrochemical hydrogen storage properties of TiPbI<sub>3</sub>/Ti<sub>4</sub>PbI<sub>6</sub> nanocomposite. *Int. J. Hydrogen Energy* 46, 6648–6658.
- Kobayakawa, K., Teranishi, A., Tsurumaki, T., Sato, Y., Fujishima, A., 1992. Photocatalytic activity of CuInS<sub>2</sub> and CuIn<sub>5</sub>S<sub>8</sub>. *Electrochim. Acta* 37, 465–467.
- Konstantinou, I.K., Albanis, T.A., 2004. TiO<sub>2</sub>-assisted photocatalytic degradation of azo dyes in aqueous solution: kinetic and mechanistic investigations: a review. *Appl. Catal. B* 49, 1–14.
- Krunks, M., Kijatkina, O., Rebane, H., Oja, I., Mikli, V., Mere, A., 2002. Composition of CuInS<sub>2</sub> thin films prepared by spray pyrolysis. *Thin Solid Films* 403, 71–75.
- Lei, K., Kou, M., Ma, Z., Deng, Y., Ye, L., Kong, Y., 2019. A comparative study on photocatalytic hydrogen evolution activity of synthesis methods of CDs/ZnIn<sub>2</sub>S<sub>4</sub> photocatalysts. *Colloids Surf., A* 574, 105–114.
- Liu, Y., Hou, C., Jiao, T., Song, J., Zhang, X., Xing, R., et al, 2018. Self-assembled AgNP-containing nanocomposites constructed by electrospinning as efficient dye photocatalyst materials for wastewater treatment. *Nanomaterials* 8, 35.
- Liu, L., Hu, R., Law, W.-C., Roy, I., Zhu, J., Ye, L., et al, 2013. Optimizing the synthesis of red-and near-infrared CuInS<sub>2</sub> and AgInS<sub>2</sub> semiconductor nanocrystals for bioimaging. *Analyst* 138, 6144–6153.
- Liu, R., Liu, Y., Liu, C., Luo, S., Teng, Y., Yang, L., et al, 2011. Enhanced photoelectrocatalytic degradation of 2, 4-dichlorophenoxyacetic acid by CuInS<sub>2</sub> nanoparticles deposition onto TiO<sub>2</sub> nanotube arrays. *J. Alloys Compd.* 509, 2434–2440.
- Luo, J., Tilley, S.D., Steier, L., Schreier, M., Mayer, M.T., Fan, H.J., et al, 2015. Solution transformation of Cu<sub>2</sub>O into CuInS<sub>2</sub> for solar water splitting. *Nano Lett.* 15, 1395–1402.
- Mahdi, M.A., Aljeboree, A.M., Jasim, L.S., Alkaim, A.F., 2021. Synthesis, characterization and adsorption studies of a graphene oxide/polyacrylic acid nanocomposite hydrogel. *NeuroQuantology* 19 (9), 46–54. <https://doi.org/10.14704/nq.2021.19.9.NQ21136>.
- Mahdiani, M., Soofivand, F., Ansari, F., Salavati-Niasari, M., 2018. Grafting of CuFe<sub>2</sub>O<sub>4</sub> nanoparticles on CNT and graphene: eco-friendly synthesis, characterization and photocatalytic activity. *J. Cleaner Prod.* 176, 1185–1197.
- Mohammed, A.H., Yousif, Q.A., 2021. A simple, step-by-step approach for the preparation of MoO<sub>3</sub>@g-C<sub>3</sub>N<sub>4</sub> nanocomposite. *J. Phys.: Conf. Ser.* 1999, 012159. <https://doi.org/10.1088/1742-6596/1999/1/012159>.
- Mu, J., Wei, Q., Yao, P., Zhao, X., Kang, S.-Z., Li, X., 2012. Facile preparation and visible light photocatalytic activity of CdIn<sub>2</sub>S<sub>4</sub> monodispersed spherical particles. *J. Alloys Compd.* 513, 506–509.
- Ong, C.B., Ng, L.Y., Mohammad, A.W., 2018. A review of ZnO nanoparticles as solar photocatalysts: Synthesis, mechanisms and applications. *Renew. Sustain. Energy Rev.* 81, 536–551.
- Orooji, Y., Ghanbari, M., Amiri, O., Salavati-Niasari, M., 2020. Facile fabrication of silver iodide/graphitic carbon nitride nanocomposites by notable photo-catalytic performance through sunlight and antimicrobial activity. *J. Hazard. Mater.* 389, 122079.
- Phaltane, S.A., Vanalakar, S., Bhat, T., Patil, P., Sartale, S., Kadam, L., 2017. Photocatalytic degradation of methylene blue by hydrothermally synthesized CZTS nanoparticles. *J. Mater. Sci.: Mater. Electron.* 28, 8186–8191.
- Rafique, M., Shaikh, A.J., Rasheed, R., Tahir, M.B., Gillani, S.S.A., Usman, A., et al, 2018. Aquatic biodegradation of methylene blue by copper oxide nanoparticles synthesized from *Azadirachta indica* leaves extract. *J. Inorg. Organomet. Polym. Mater.* 28, 2455–2462.
- Regulacio, M.D., Han, M.-Y., 2016. Multinary I-III-VI<sub>2</sub> and I<sub>2</sub>-II-IV-VI<sub>4</sub> semiconductor nanostructures for photocatalytic applications. *Acc. Chem. Res.* 49, 511–519.
- Schneider, J., Matsuoka, M., Takeuchi, M., Zhang, J., Horiuchi, Y., Anpo, M., et al, 2014. Understanding TiO<sub>2</sub> photocatalysis: mechanisms and materials. *Chem. Rev.* 114, 9919–9986.
- Soylak, M., Erdogan, N.D., 2006. Copper(II)-rubeanic acid coprecipitation system for separation–preconcentration of trace metal ions in environmental samples for their flame atomic absorption spectrometric determinations. *J. Hazard. Mater.* 137, 1035–1041.
- Sun, M., Zhao, X., Zeng, Q., Yan, T., Ji, P., Wu, T., et al, 2017. Facile synthesis of hierarchical ZnIn<sub>2</sub>S<sub>4</sub>/CdIn<sub>2</sub>S<sub>4</sub> microspheres with enhanced visible light driven photocatalytic activity. *Appl. Surf. Sci.* 407, 328–336.
- Sunayana, S., Nitin, C., Chaturvedi, R., Sharma, M., 2010. Photocatalytic degradation of eriochrome black T using ammonium phosphomolybdate semiconductor. *Int. J. Chem. Sci.* 8, 1580–1590.
- Tahir, M.B., Sagir, M., Zubair, M., Rafique, M., Abbas, I., Shakil, M., et al, 2018. WO<sub>3</sub> nanostructures-based photocatalyst approach towards degradation of RhB dye. *J. Inorg. Organomet. Polym. Mater.* 28, 1107–1113.

- Tang, J., Li, D., Feng, Z., Tan, Z., Ou, B., 2014. A novel AgIO<sub>4</sub> semiconductor with ultrahigh activity in photodegradation of organic dyes: insights into the photosensitization mechanism. *RSC Adv.* 4, 2151–2154.
- Thwin, M., Mahmoudi, B., Ivaschuk, O.A., Yousif, Q.A., 2019. An efficient and recyclable nanocatalyst for the green and rapid synthesis of biologically active polysubstituted pyrroles and 1,2,4,5-tetrasubstituted imidazole derivatives. *RSC Adv.* 9, 15966–15975. <https://doi.org/10.1039/c9ra02325a>.
- Xu, H., Zhang, W., Jin, W., Ding, Y., Zhong, X., 2013. Facile synthesis of ZnS–CdIn<sub>2</sub>S<sub>4</sub>-alloyed nanocrystals with tunable band gap and its photocatalytic activity. *J. Lumin.* 135, 47–54.
- Yousif, Q.A., 2021. Environmentally sustainable disposal of expired albendazole medication and its role in the protection of mild steel. *IOP Conf. Ser.: Earth Environ. Sci.* 790,. <https://doi.org/10.1088/1755-1315/790/1/012072> 012072.
- Yousif, Q.A., Agbolaghi, S., 2020. A Comparison Between Functions of Carbon Nanotube and Reduced Graphene Oxide and Respective Ameliorated Derivatives in Perovskite Solar Cells. *Macromol. Res.* 28, 425–432. <https://doi.org/10.1007/s13233-020-8054-8>.
- Yousif, Y.Q.A., Al-Zhara, A.A., 2016. Electrochemical methods, sem-eds and afm studies for assessing corrosion inhibition of carbon steel in acidic media. *ARN J. Eng. Appl. Sci.* 11, 12619–12630.
- Yousif, Q.A., Haran, N.H., 2021. Fabrication of TiO<sub>2</sub> nanotubes via three-electrodes anodization technique under sound waves impact and use in dye-sensitized solar cell. *Egypt. J. Chem.* 64, 125–132. <https://doi.org/10.21608/EJCHEM.2020.28233.2596>.
- Yuan, D., Sun, M., Zhao, M., Tang, S., Qi, J., Zhang, X., et al, 2020. Persulfate promoted ZnIn<sub>2</sub>S<sub>4</sub> visible light photocatalytic dye decomposition. *Int. J. Electrochem. Sci.* 15, 8761–8770.
- Zhang, J., Song, H., Cui, R., Deng, C., Yousif, Q.A., 2020. SCMNPs@Urea/Py-CuCl<sub>2</sub>: a recyclable catalyst for the synthesis of pyrano[2,3-d]pyrimidinone and pyrano[2,3-d] pyrimidine-2,4,7-trione derivatives. *J. Coord. Chem.* 73, 558–578. <https://doi.org/10.1080/00958972.2020.1737681>.
- Zhang, H., Zhu, Y., 2010. Significant visible photoactivity and antiphotocorrosion performance of CdS photocatalysts after monolayer polyaniline hybridization. *J. Phys. Chem. C* 114, 5822–5826.